ANL-HEP-PR-97-21
UFIFT-HEP-97-12
JLAB-THY-97-40

Rapidity Correlations and ΔG from Prompt Photon plus Jet Production in Polarized pp Collisions

Sanghyeon Chang[1*], Claudio Corianò[2†] *and* L. E. Gordon[3 ‡]
[1] *Institute for Fundamental Theory, Phys. Dept., Univ. of Florida, Gainesville, FL 32611*
[2] *Theory Group, Jefferson Lab, Newport News, VA 23606*
[3] *High Energy Physics Division, Argonne National Laboratory, Argonne, IL 60439, USA*

Abstract

A study of prompt photon plus associated jet production is performed at next-to-leading order ($O(\alpha\alpha_s^2)$) in QCD at $\sqrt{S} = 200 - 500$ GeV, appropriate for the RHIC polarized $\vec{p}\vec{p}$ collider experiment. Momentum correlations between the jet and photon are examined and the utility of the process as a method for constraining the size and shape of the polarized gluon density of the proton ΔG is examined.

I. INTRODUCTION

With the advent of RHIC, the Relativistic Heavy Ion Collider at Brookhaven, QCD will enter into a new interesting phase in which polarized high energy collisions will become a standard tool of analysis in high energy physics. RHIC, as a pp collider, will be endowed with a very high luminosity (500 pb^{-1}), not easily accessible to $p\bar{p}$ colliders and will be spanning a center of mass energy range between 50 to 500 GeV.

One of the main programs at RHIC will be to nail down the size and the shape of the polarized parton distributions which, at the moment, suffer from significant model dependence, especially in the gluon contribution (ΔG). Interest in spin physics has grown in the last few years thanks to the various polarized DIS experiments and to the existing proposal for the construction of a pp collider at DESY (HERA-$\vec{N}$) running at lower energy (≈ 50 GeV).

*E-mail address: schang@phys.ufl.edu

†E-mail address: coriano@jlabs2.jlab.org

‡E-mail address: gordon@hep.anl.gov

More generally, besides the important information on the spin structure of the nucleon which can be gathered from these experiments, it is obvious that one might try to look for physics beyond the Standard Model using polarization as a tool to suppress unwanted background and to enhance specific signals. The studies of chiral couplings in the Standard Model or even compositeness will require precise measurements of the hadronic background. There have been many attempts in the last few years at creating a backbone-program for RHIC by analyzing a set of processes in leading order and by defining suitable observables which are more easily accessible to the experimental investigations.

More recently, next to leading order (NLO) studies of various processes (see for instance [1]) have been presented. A partial review of these developments can be found in [2]. Among the most interesting processes which require an accurate theoretical determination are single and double prompt photon production, single and 2-jet production and the Drell-Yan lepton-pair production. Work on the Drell Yan cross section at NLO has been presented [3,4], limited at the moment to the non-singlet sector, which is sensitive to the polarization of the quark distributions. Due to the fact that the initial partons are longitudinally (or transversely) polarized, the calculation of the hard scatterings are far more involved than in the unpolarized case.

Although the studies of the *total* cross sections for some of these and other related processes will be necessary in order to guarantee experimental observability of the cross sections and thus the spin asymmetries, which are usually estimated to be small, the study of the event-structure of these processes can provide interesting new insights into the spin distributions. In this paper we study and compare the structure of prompt photon plus single jet production in the polarized and unpolarized cases at RHIC center-of-mass energies.

II. MONTE CARLO CALCULATIONS AT NLO

Compared to total cross sections, distributions usually reveal more detail about the underlying hard scattering mechanisms as well as more information on the x-dependence of the model structure functions. The drawback is that they are generally more difficult to define theoretically to NLO, since many of them are affected by non-canceling infrared divergences. Modern developments in combined Analytic/Monte Carlo techniques allow to get exact numerical results for the NLO corrections in a reasonable amount of time. In addition they allow great flexibility in placing experimental selections such as jet definitions and photon isolation cuts on the cross sections, thereby allowing a more realistic and direct comparison with data.

The analytical part of the calculation involves the 1) exact (analytical) evaluation of the virtual corrections and 2) the exposure (by a cutoff regularization) of all the mass singularities in the real emissions. The rest of the phase space is then integrated over numerically. We omit a general presentation of the method which can be found elsewhere and focus on the study at NLO of the rapidity correlations in photon plus associated jet production.

In the next sections, after a brief overview of the various contributions to the cross section, we move to a study of the rapidity correlations between the photon and the jet. The analysis presented is similar in spirit to the study of momentum correlation given in ref . [5,6], with the due modifications.

III. THE PHOTON PLUS JET CROSS SECTION

The main goal at polarized hadron colliders is the study of the polarized parton distributions of the nucleon which are defined by

$$\Delta f_i(x, M^2) = f_i^+(x, M^2) - f_i^-(x, M^2). \tag{3.1}$$

The corresponding unpolarized distributions are defined by

$$f_i(x, M^2) = f_i^+(x, M^2) + f_i^-(x, M^2), \tag{3.2}$$

where f_i^+ and f_i^- represent the distribution of partons of type i with positive and negative helicities respectively, with respect to that of the parent hadron. The hard subprocess scattering cross sections are defined by

$$\Delta\hat{\sigma}_{ij} = \frac{1}{2}\left(\sigma^{++} - \sigma^{+-}\right) \tag{3.3}$$

and

$$\hat{\sigma}_{ij} = \frac{1}{2}\left(\sigma^{++} + \sigma^{+-}\right). \tag{3.4}$$

for the polarized and unpolarized cases respectively.

It has been observed by many authors that the cross section for prompt photon production is dominated by the subprocess $qg \to \gamma q$ in hadronic collisions already in leading order. This means that the cross section, if properly understood, could potentially prove very useful for providing information on the unpolarized gluon densities, $g(x, Q^2)$, of hadrons. Original Born level studies of this cross section also indicated that the same is true in the polarized case. It has therefore been suggested that it may prove useful in pinning down the polarized gluon densities [7]. In this context it has been examined quite extensively in leading, and more recently in next-to-leading order [8] [9]. The most recent NLO study [10] included the effects of photon isolation on the cross section. The results of all the NLO studies confirmed the conclusions from the LO ones that the cross section is very sensitive to ΔG and that the asymmetries are perturbatively stable.

Recently the photon plus jet cross section was studied in LO [11] and NLO [12] and HERA-$\vec{\text{N}}$ cms energies. The main conclusions from these studies is that this cross section will give more detail about the x-shape of the polarized gluon distribution than the single prompt photon cross section. The present calculation follows along the same lines as that in ref. [12] and we therefore do not give more detail about the contributing subprocesses here, except to say that the fragmentation contributions are estimated in LO here as well. In the present case, before isolation, these contributions are numerically more important due to the higher cms energy of the RHIC collider. The results of ref. [10] also showed that isolation significantly reduced these contributions and that that their presence, although affecting the predictions for the cross sections, did not affect the asymmetries very much.

A. Rapidity Correlations to LO and NLO

As mentioned above, although single inclusive prompt photon production will definitely be very important for constraining the size of ΔG, information on the detailed x-shape of the distribution will not be as easily extracted. This is because the calculation of the inclusive cross section involves one convolution over the momentum fractions, x, of the initial partons. In fact, at hadron level, the factorized hadronic total cross section is generically denoted as

$$\Delta\sigma = \sum_{i,j} \int_0^1 dx_1 dx_2 \Delta f_i(x_1,) \Delta f_j(x_2) \int d\Delta\sigma. \tag{3.5}$$

where we sum over all the partons i, j. The practical effect of the integral over the x_i is that a measurement of the kinematic variables of the photon is not sufficient to determine them. If, on the other hand, one or more of the jets produced in the reaction is also tagged, no convolution is involved in the calculation and the cross section is directly proportional to the parton densities.

The cross section of interest here is the triple differential cross section

$$\frac{d^3\Delta\sigma^{\gamma J}}{dp_T^\gamma d\eta^\gamma d\eta^J},$$

where η^γ and η^J are the pseudorapidities of the photon and jet respectively and p_T^γ is the transverse momentum of the photon.

We use light-cone coordinates

$$p_1 = p_1^+ n^+ = x_1 Q n^+ \qquad p_2 = p_2^- n^- = x_2 Q n^- \qquad n^\pm = 1/\sqrt{2}(1, \mathbf{0}\perp, \pm\mathbf{1})$$

with $Q = \sqrt{S}/2$ denoting the $\pm$ components on the light cone of the two incoming hadrons of momenta P_1 and P_2. We also set $p_1 = x_1 P_1$ and $p_2 = x_2 P_2$ for the two partons that enter the hard scattering.

The 4-dimensional δ function and the integration variables k_i are also rewritten on the light cone ($k_i = k_i^+, k_i^- k_{i\perp}$) and after simple manipulations we get

$$\Delta\sigma \sim \sum_{ij} \int_0^1 dx_1 \int_0^1 dx_2 \Delta f_i(x_1) \Delta f_j(x_2) \int dk_1^+ dk_2^- d^2k_{1\perp} \delta(k_1^2)\delta(k_2^2)\Delta|M|^2. \tag{3.6}$$

We have set

$$k_1^+ = \frac{k_\perp}{\sqrt{2}} e^{y_1} \qquad k_2^- = \frac{k_\perp}{\sqrt{2}} e^{-y_2}. \tag{3.7}$$

We have defined the two rapidities

$$y_i = \frac{1}{2} \log \frac{k_i^+}{k_i^-} \qquad i = 1, 2 \tag{3.8}$$

and introduced the rapidity difference $\Delta y = y_1 - y_2$.

We easily get

$$\frac{d^3\Delta\sigma^{\gamma J}}{dp_T^\gamma d\eta^\gamma d\eta^J} \equiv \frac{d\Delta\sigma}{dk_\perp dy_1 dy_2} = 2k_\perp \overline{x_1 x_2} \sum_{ij} \Delta f_i(\overline{x_1}) \Delta f_j(\overline{x_2}) \frac{d\Delta\sigma}{dt} \tag{3.9}$$

A derivation of this result is illustrated in the appendix. A similar result applies to the unpolarized case, except that the polarized cross sections and structure functions are replaced by the corresponding unpolarized ones. In this next-to-leading order calculation a jet definition is required. Throughout we use the Snowmass [18] jet definition.

All the 2-to-2 contributions (Born and virtual) to the photon-plus-jet cross section give contributions with structure functions sampled at fixed kinematical points x_i. Thus the double longitudinal asymmetry A_{LL}, defined as the ratio of the polarized to the unpolarized cross section, is directly proportional to the ratio $\Delta G/g$ [11] in kinematic regions where other subprocesses such as $q\bar{q}$ scattering can be neglected. This guarantees sensitivity of the asymmetries to ΔG.

IV. RESULTS

All results are displayed for $\vec{p}\vec{p}$ collisions at the center-of-mass energy $\sqrt{s} = 200$ and 500 GeV which are energies typical for the RHIC experiment at Brookhaven. For the unpolarized cross section the CTEQ4M parton densities [13] are used throughout, and the value of $\Lambda_{\overline{MS}}$ corresponding to this distribution is also used. Use of other unpolarized parton densities at the x-values probed here do not yield significantly different results. For the polarized case the GRSV [14] and GS [15] distributions are used with the corresponding values for $\Lambda_{\overline{MS}}$. The authors of ref. [14] and [15] have proposed various parameterizations of the polarized parton densities differing mainly in the choice of input for the polarized gluon density ΔG. In the case of the GRSV distributions we use the 'valence' set which corresponds to a fit of the available DIS data (referred to by the authors as the 'fitted' ΔG scenario), the large gluon fit which assumes that $\Delta G(x, Q_0^2) = g(x, Q_0^2)$ at input (the '$\Delta G = g$' scenario) and the small gluon fit which uses $\Delta G(x, Q_0^2) = 0$ at the input scale (the '$\Delta G = 0$' scenario), which in this case starts at the very low value of $Q_0^2 = 0.34$ GeV^2. The latter two distributions are intended to represent extreme choices for ΔG. These parameterizations give gluon densities which differ in their absolute sizes as well as in their x-shape. The GS parameterizations provide three fits to the data; GS A, GS B and GS C. It has been shown that the GS A and GS B distributions do not differ very much from the $\Delta G = g$ and fitted ΔG sets of GRSV respectively, whereas the the GS C set is widely different from any of the others. We shall present distributions using the three GRSV sets discussed above, along with the GS C set for comparison. For the fragmentation functions we use the LO asymptotic parameterization of ref. [16]. As will be shown, the choice of fragmentation functions makes very little difference to the predictions, since these processes account for only a small fraction of the cross section.

The renormalization, factorization, and fragmentation scales are set to a common value $\mu = p_T^\gamma$ unless otherwise stated. Since there are two 'particles' in the final state, the jet and the photon, both of whose transverse momenta are large, an alternative choice might be $\mu = p_T^J$ or some function of p_T^γ and p_T^J. The results of the calculations show that the magnitudes of p_T^γ and p_T^J tend to be comparable and that dependence of the asymmetries on μ is slight, although the individual cross sections may vary significantly with μ. Therefore, choices of μ different from $\mu = p_T^\gamma$ should not produce significantly different predictions

for the asymmetries . The two loop expression for $\alpha_s(Q^2)$ is used throughout, with the number of flavors fixed at $N_f = 4$, although the contribution from charm was verified to be negligible at the energies considered and is not included. None of the currently available polarized distributions include a parameterization of the charm quark distribution. A new NLO parameterization is in preparation which includes charm, but is not yet available for this study [17]. Finally, the values of both the jet cone size and photon isolation cones are fixed at $R_J = 0.7$ and $r_\gamma = 0.7$ respectively, unless otherwise stated.

Figs.1a and b show the triple differential cross section as a function of p_T^γ of the photon for the various parameterizations at $\sqrt{S} = 500$ and 200 GeV respectively. The unpolarized cross sections are shown for comparison. The curves were obtained by averaging over bins $\Delta p_T^\gamma = 1$ GeV and the restriction $p_T^J \geq 10$ GeV was imposed. In addition both the photon and jet rapidities are averaged over the central region, $-0.5 \leq \eta^\gamma, \eta^J \leq 0.5$. All the parameterizations give distributions which are distinctly different in both their shapes and sizes. Their relative sizes are in direct relation to the sizes and shapes of their respective gluon distributions. This is most obvious for the GS C parameterization which has the most distinct gluon distribution, being negative over part of the x-range. The curves show a rise between $p_T^\gamma = 10$ and 11 GeV because of the restriction $p_T^J \geq 10$ GeV and the fact that the bin centered at 10 GeV is averaged over the range $9.5 \leq p_T^\gamma \geq 10.5$ GeV. Above $p_T^\gamma = 10$ GeV both the two- and three-body contributions to the cross section are finite whereas below this value, only the latter are finite since the two-body contributions always produce a photon balancing the p_T of the jet.

Figs.1c and 1d show the asymmetries for 1a and 1b respectively. There are clear distinctions between the predictions for the various parameterizations which will certainly make them distinguishable in the experiments. As expected, at the lower $\sqrt{S}$ the asymmetries are larger, but the corresponding cross sections are smaller. Combining both sets of results will nevertheless suggests that a measurement of the polarized gluon distribution will be possible between $x = 0.04$ and $x = 0.5$.

In Figs.2a and 2b we look at distributions in η^γ at $p_T^\gamma = 10$ GeV with the restriction $p_T^J \geq 10$ GeV still imposed. In both cases $\sqrt{S} = 200$ GeV. In Fig.2a the jet is restricted to be in the central rapidity region, $-0.5 \leq \eta^J \leq 0.5$, and in Fig.2c it is restricted to the forward region, $0.5 \leq \eta^J \leq 1.5$. The textures of the different curves follow the same conventions as in figs.1a-d. A visual comparison of the figures show clearly that when the jet is in the central rapidity region the, the photon rapidity distribution peaks at $\eta^\gamma = 0$, whereas when the jet is restricted to the forward rapidity region, the η^γ also peaks in this region. This positive rapidity correlation between the photon and jet is present for both the polarized and unpolarized cross sections although it is clearly stronger in the unpolarized case.

Fig.2c which shows the corresponding asymmetries for the curves in fig.2a, verifies that the distributions are symmetric and also shows that they have distinctive shapes. The corresponding asymmetry curves for fig.2b all rise sharply in the negative rapidity region, i.e., in the opposite direction to the region where the rapidity distributions peak. Thus the asymmetries display a negative rapidity correlation between the photon and jet. An explanation for this behavior was given in ref. [12] in terms of competing effects between the subprocess matrix elements, which tend generate positive rapidity correlations, and the polarized parton distributions which tend to produce negative correlations.

In figs.3a and 3b rapidity distributions are plotted for the jet using similar cuts to those

used in figs.2a and 2b. In fig.3a, the photon is restricted to be in the central rapidity region whereas in 3b it is restricted to be in the forward region. As before, there is a net positive rapidity correlation between the photon and jet for the polarized as well as the unpolarized cases, but as fig.3d shows, the effect is stronger for the unpolarized case. This leads the asymmetries to peak at negative rapidities of the jet.

One of the striking features of the asymmetry curves in figs.3c and 3d is the differences in their shapes as compared to each other and as compared to those of figs.2c and 2d. The parameterizations with the larger polarized gluon distributions the "fitted" ΔG and $\Delta G = g$ scenarios give asymmetries which decrease as η^J moves away from the central region in fig.3c and away from $\eta^J \sim -1.5$ in fig.3d. The differences between these curves and those of fig.2 are explained by the asymmetric p_T cuts between the photon and jet which affects the phase space available for jet or prompt photon production differently.

The differences between the shapes of the asymmetries for the various models of polarized parton distributions in figs.3c and 3d are due to the differences in the x-shapes of the polarized parton distributions, particularly those for ΔG. All the asymmetries fall as η^J goes to the extreme values as may be expected since the unpolarized gluon distribution has a singular (x^{-a} where $a < 1$) behaviour at small x, whereas all the polarized gluon distributions go to zero at small x. All the other differences between the asymmetries are due directly to the differences between the corresponding polarized parton distributions. This re-enforces the conclusion that this cross section will undoubtedly yield very important information on the polarized parton distributions.

V. CONCLUSIONS

We have examined the possibility that both the size and x-shape of the polarized gluon distribution of the proton, ΔG, may be measured at RHIC via a measurement of the photon plus jet cross section. Control over the kinematic variables of both the photon and jet allows a much better determination of the x-value probed when compared to inclusive prompt photon production. A comparison of the predictions obtained using different polarized parton densities show that a clear distinction between both the sizes and shapes should be possible. Further more detailed information on the x-shapes of the polarized gluon distribution will be obtainable by carefully choosing the kinematic regions in which the jet and/or photon is tagged.

Assuming that the 'fitted ΔG' scenario is the most plausible distribution, then a typical value for the asymmetry, A_{LL} is 5%, but given the uncertainty in ΔG the asymmetry could be as small as 1% or as large as 20%. The expected small-x behavior of the polarized and unpolarized distributions lead to differencs in correlations between the rapidities of the photon and jet in each case. This effect can produce very large asymmetries in certain regions of phase space which may be expolited and used to discriminate between various models of ΔG.

VI. APPENDIX

The cross section for the 2-to-2 process is generically given by

$$d\sigma = \frac{|M|^2(2\pi)^4}{4p_1\cdot p_2}\delta^4(p_1+p_2-k_1-k_2)\frac{\delta_+(k_1^2)}{(2\pi)^3}\frac{\delta_+(k_2)^2}{(2\pi)^3}\delta^4(p_1+p_2-k_1-k_2), \tag{6.1}$$

and working in the c.m frame

$$\frac{d\sigma}{d\,t} = \frac{1}{16\pi^2}|M|^2. \tag{6.2}$$

We expand the final state momenta in the light cone variables

$$\begin{aligned}\sigma \sim \int dk_1^+ dk_1^- d^2k_{1\perp} dk_2^+ dk_2^- d^2k_{2\perp}\delta^{(2)}(k_{1\perp}+k_{2\perp})\delta(p_1^+ + p_2^+ - k_1^+ - k_2^+)\\ \times\delta(p_1^- + p_2^- - k_1^- - k_2^-)\delta_+(k_1^2)\ \delta_+(k_2^2)\end{aligned} \tag{6.3}$$

and integrate over k_1^-, k_2^+ and $k_{2\perp}$, thereby eliminatigng 3 of the 5 delta functions.

The remaining 2 delta functions are rewritten as

$$\begin{aligned}\delta(k_1^2) &= \delta\left(\sqrt{2}k_\perp e^{y_1}(x_2Q - k_\perp e^{-y_2}) - k_\perp^2\right)\\ \delta(k_2^2) &= \delta\left(\sqrt{2}k_\perp e^{-y_2}(x_1Q - k_\perp e^{y_1}) - k_\perp^2\right)\end{aligned} \tag{6.4}$$

and the integration over the parton fractions $x_1,\ x_2$ performed by the relation

$$\delta_+(k_1^2)\ \delta_+(k_2^2) = \frac{1}{2k_\perp^2 e^{\Delta y}Q^2}\delta(x_1-\overline{x}_1)\delta(x_1-\overline{x}_2) \tag{6.5}$$

with

$$\begin{aligned}\overline{x}_1 &= \frac{k_\perp(1+e^{\Delta y})}{\sqrt{2}Qe^{y_1}}\\ \overline{x}_2 &= \frac{k_\perp(1+e^{\Delta y})}{\sqrt{2}Qe^{-y_2}}.\end{aligned} \tag{6.6}$$

Therefore, the convolution integral for the cross section is reorganized as follows

$$\begin{aligned}d\sigma &\sim \int_0^1 dx_1\int_0^1 dx_2 f(x_1)f(x_2)\int dk_1^+ dk_2^- d^2k_\perp\delta(k_1^2)\delta(k_2^2)|M|^2\\ &= \int_0^1 dx_1\int_0^1 dx_2 f(x_1)f(x_2)\int dk_1^+ dk_2^- d^2k_\perp\frac{\delta(x_1-\overline{x}_1)\delta(x_1-\overline{x}_2)}{2k_\perp^2 e^{\Delta y}Q^2}|M|^2\\ &= f(\overline{x}_1)f(\overline{x}_2)\int\frac{dk_1^+ dk_2^- d^2k_\perp}{2|k_\perp|^2 e^{\Delta y}Q^2}.\end{aligned} \tag{6.7}$$

At this point we change the remaining integration variables to the rapidity space using $\partial(k_1^+,k_2^-)/\partial(y_1,y_2) = exp[\Delta y]k_\perp^2/2$ and perform the integration over one of the angle in $\vec{k}_\perp$. With the correct normalization, we get the result in 3.9.

VII. ACKNOWLEDGMENTS

The work at Argonne National Laboratory was supported by the US Department of Energy, Division of High Energy Physics, Contract number W-31-109-ENG-38.

REFERENCES

[1] C. Corianò and L. E. Gordon, Nucl.Phys.B469 (1996) 202.

[2] H.-Y. Cheng, Int. Journal of Modern Physics **A**, Vol.11, N0.29 (1996) 5109

[3] S. Chang, C. Corianò, R. D. Field and L. E. Gordon, Phys. Lett. B403 (1997) 344, hep/ph 9705249, submitted to Nucl. Phys. B.

[4] S. Chang, C. Corianò and J. K. Elwood, UFIFT-HEP-97-25.

[5] E. L. Berger, Phys. Rev. **D37** (1988) 1810.

[6] B. Bailey, E. L. Berger and L. E. Gordon, Phys. Rev. **D54** (1996) 1896.

[7] E. L. Berger and J. Qiu Phys. Rev. **D40**, 778 (1989).

[8] A. P. Contogouris, B. Kamal, Z. Merebashvili and F. V. Tkachov, Phys. Lett. **B304** 329 (1993); Phys. Rev. **D48** 4092 (1993).

[9] L. E. Gordon and W. Vogelsang, Phys. Rev. **D48**, 3136 (1993) and **D49**, 170 (1994).

[10] L. E. Gordon, ANL-HEP-PR-96-100 (to be published Nucl. Phys. B).

[11] W.-D. Nowak "Possible Measurements of Single and Double Spin Asymmetries with HERA-$\vec{\text{N}}$" DESY-96-095.

[12] L. E. Gordon, ANL-HEP-PR-96-78 (to be published Phys. Lett. B).

[13] CTEQ Collaboration, H. L. Lai *et al.,* Phys. Rev. D51, 4763 (1995).

[14] M. Glück, E. Reya, M. Stratman and W. Vogelsang, Phys. Rev. **D53**, 4775 (1996).

[15] T. Gehrmann and W. J. Stirling, Phys. Rev. **D53**, 6100 (1996).

[16] J. F. Owens, Phys. Rev. **D26** (1982) 1600.

[17] G. P. Ramsey, Prog.Part.Nucl.Phys.39 (1997) 599

[18] J. Huth *et. al.,* Proc. of the 1990 DPF Summer Study on High Energy Physics, Snowmass, Colorado, ed. E. L. Berger, World Scientific, 1992, p. 134.

FIGURE CAPTIONS

[1] (a) p_T^γ distribution of the photon plus jet triple differential cross section $d^3\sigma^{\gamma J}/dp_T^\gamma d\eta^\gamma d\eta^J$ at $\sqrt{S} = 500$ GeV for various polarized parton distributions and for rapidities of the photon and jet averaged over the region $-0.5 \leq \eta^\gamma, \eta^J \leq 0.5$. The cut $p_T^J \geq 10$ GeV is imposed. (b) Similar to (a) at $\sqrt{S} = 200$ GeV. (c) and (d) Corresponding asymmetries for the distributions in (a) and (b) respectively.

[2] (a) Distribution in the rapidity of the photon at $p_T^\gamma = 10$ GeV and η^J averaged over the region $-0.5 \leq \eta^J \leq 0.5$ and $p_T^J \geq 10$ GeV at $\sqrt{S} = 200GeV$. (b) Similar to (a) but for $0.5 \leq \eta^J \leq 1.5$. (c) and (d) Asymmetries for the curves shown in (a) and (b) respectively.

[3] (a) Distribution in the rapidity of the jet at $p_T^\gamma = 10$ GeV and η^γ averaged over the region $-0.5 \leq \eta^\gamma \leq 0.5$ and $p_T^J \geq 10$ GeV at $\sqrt{S} = 200GeV$. (b) Similar to (a) but for $0.5 \leq \eta^\gamma \leq 1.5$. (c) and (d) Asymmetries for the curves shown in (a) and (b) respectively.

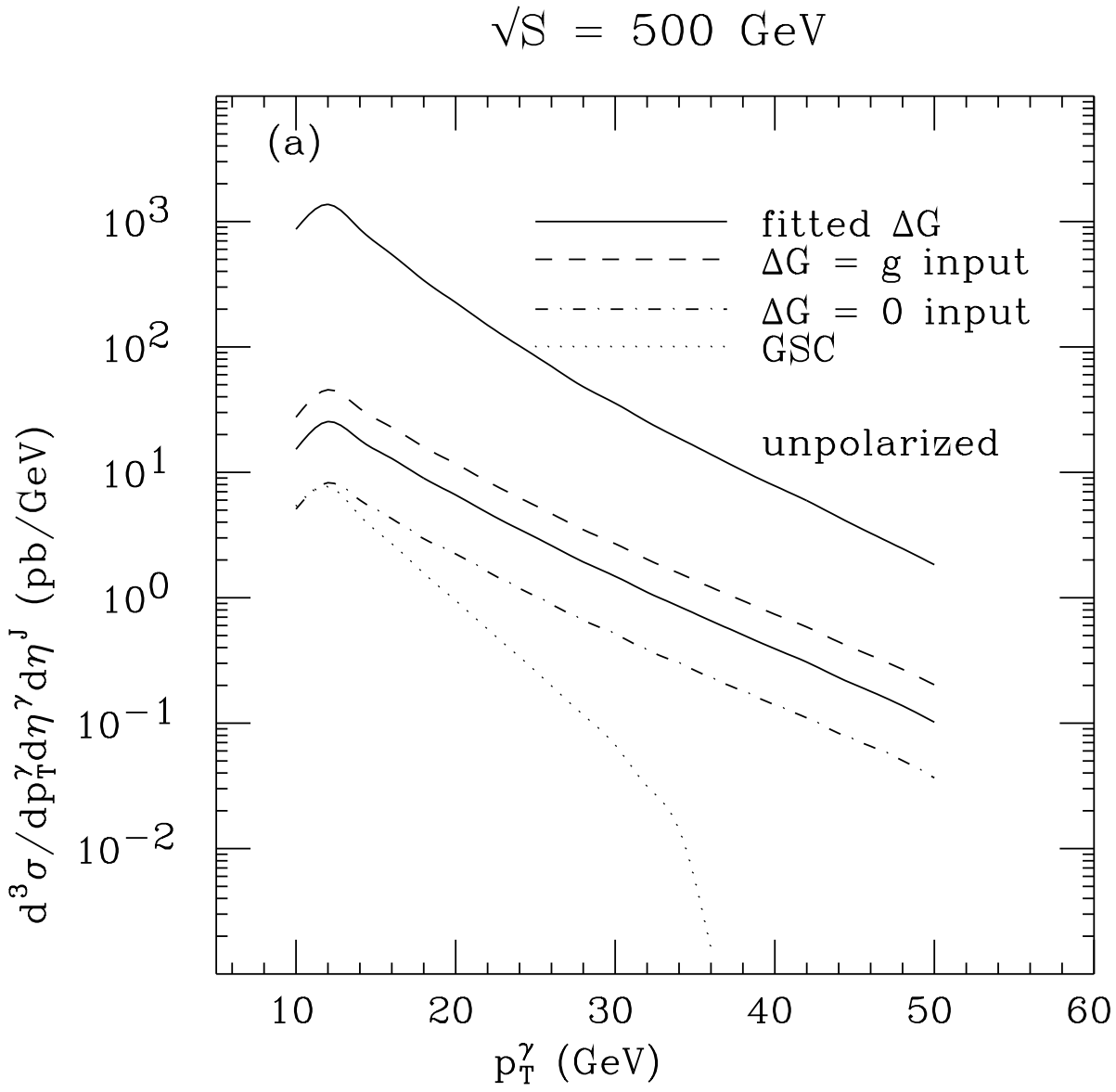
√S = 500 GeV
(a)
fitted ΔG
ΔG = g input
ΔG = 0 input
GSC
unpolarized
10^3
10^2
10^1
10^0
10^{-1}
10^{-2}
$d^3\sigma/dp_T^\gamma d\eta^\gamma d\eta^J$ (pb/GeV)
10
20
30
40
50
60
p_T^γ (GeV)

Fig. 1a

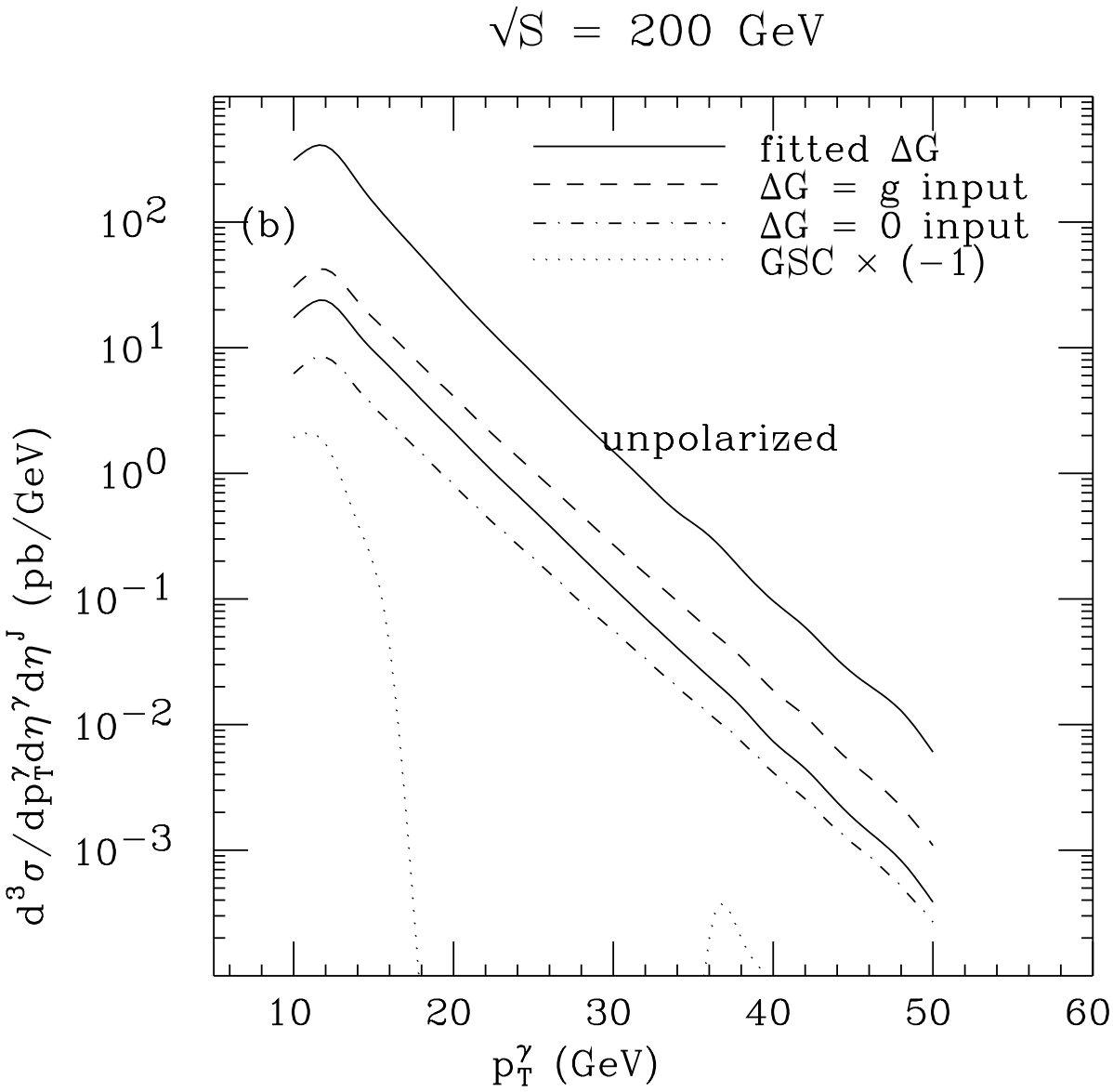
√S = 200 GeV
(b)
fitted ΔG
ΔG = g input
ΔG = 0 input
GSC × (−1)
unpolarized
10^2
10^1
10^0
10^{-1}
10^{-2}
10^{-3}
$d^3\sigma/dp_T^\gamma d\eta^\gamma d\eta^J$ (pb/GeV)
10
20
30
40
50
60
p_T^γ (GeV)

Fig. 1b

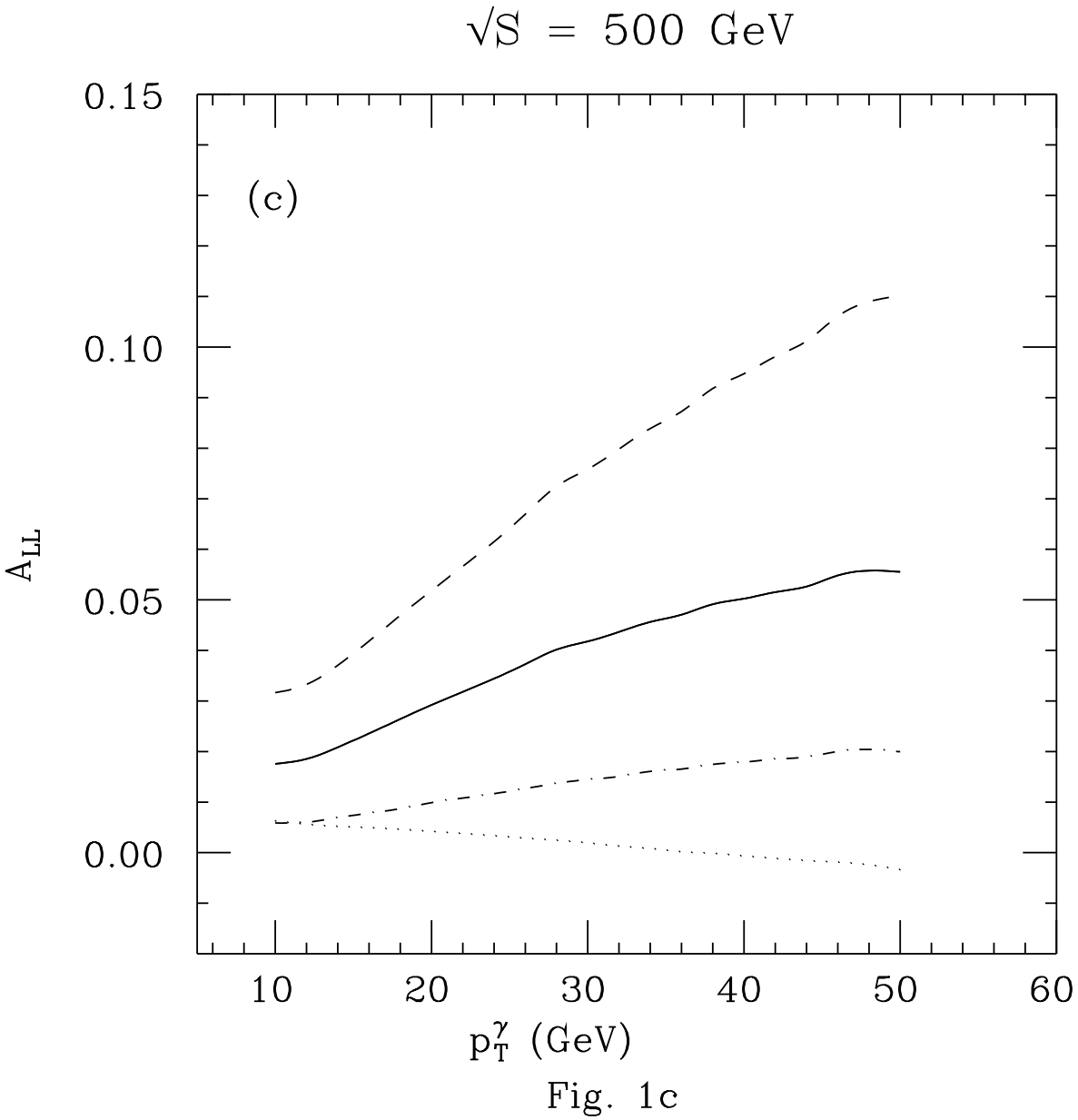

Fig. 1c

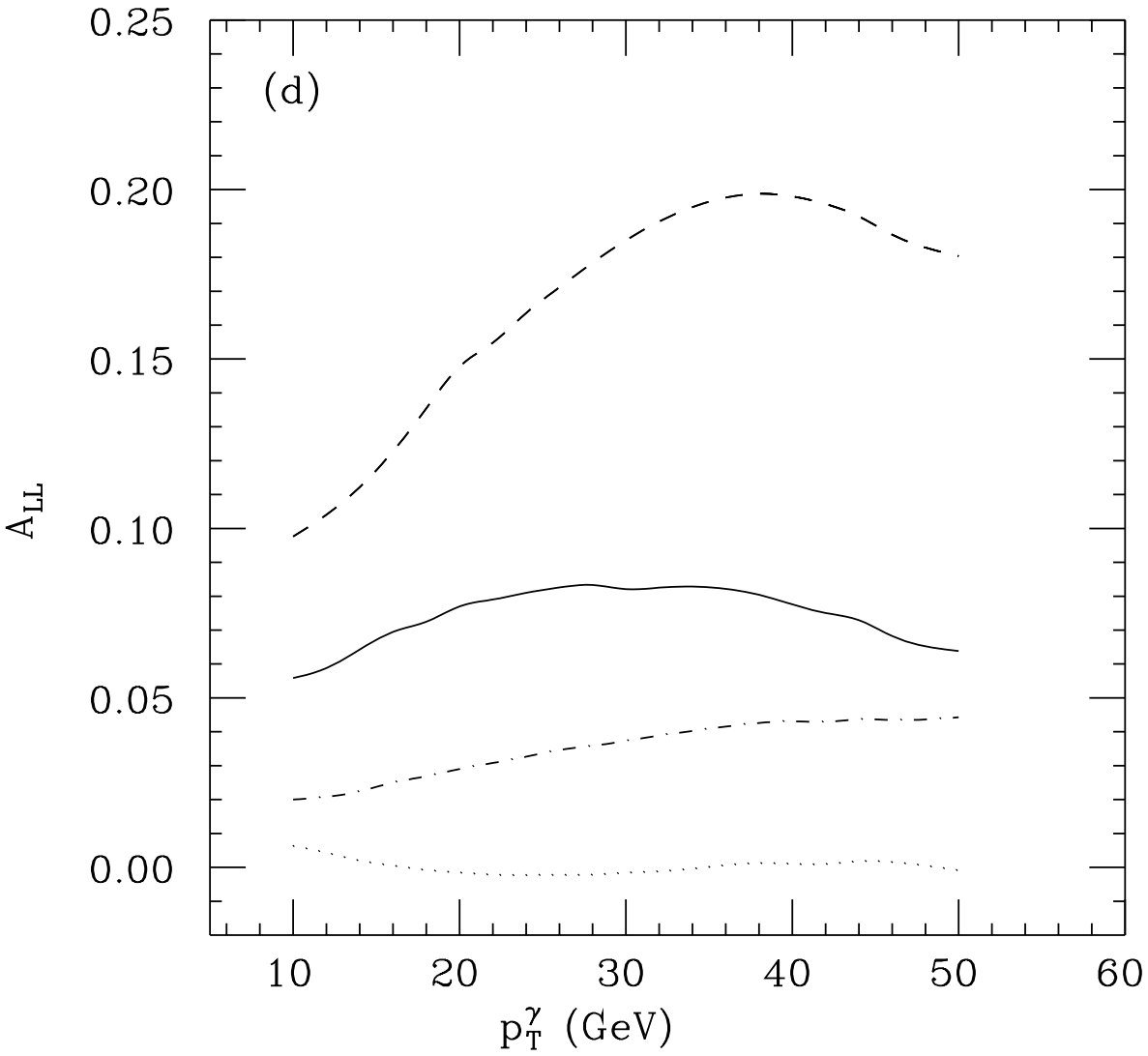

Fig. 1d

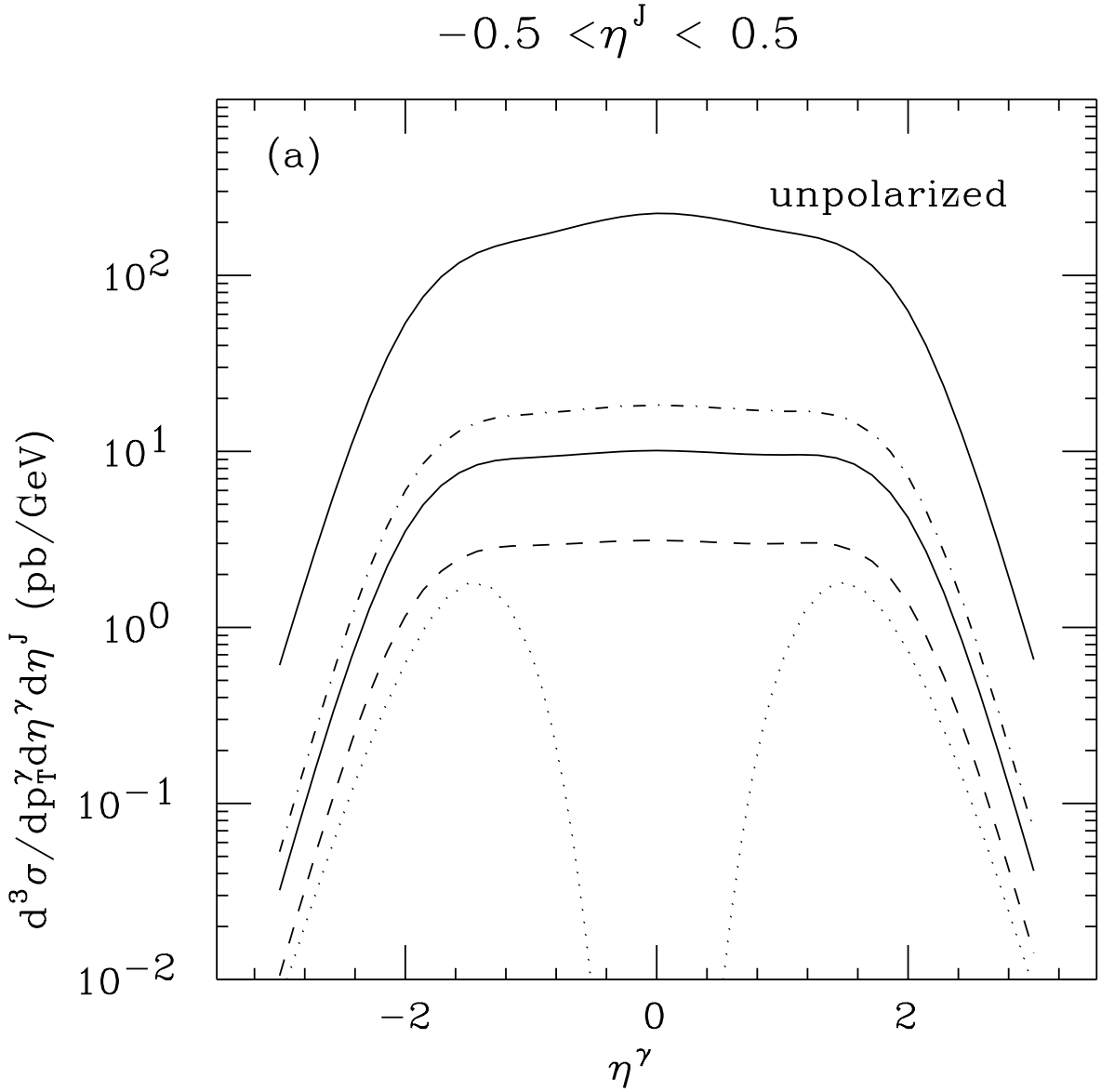
$-0.5 < \eta^J < 0.5$
(a)
unpolarized
10^2
10^1
10^0
10^{-1}
10^{-2}
$d^3\sigma/dp_T^\gamma d\eta^\gamma d\eta^J$ (pb/GeV)
−2
0
2
η^γ

Fig. 2a

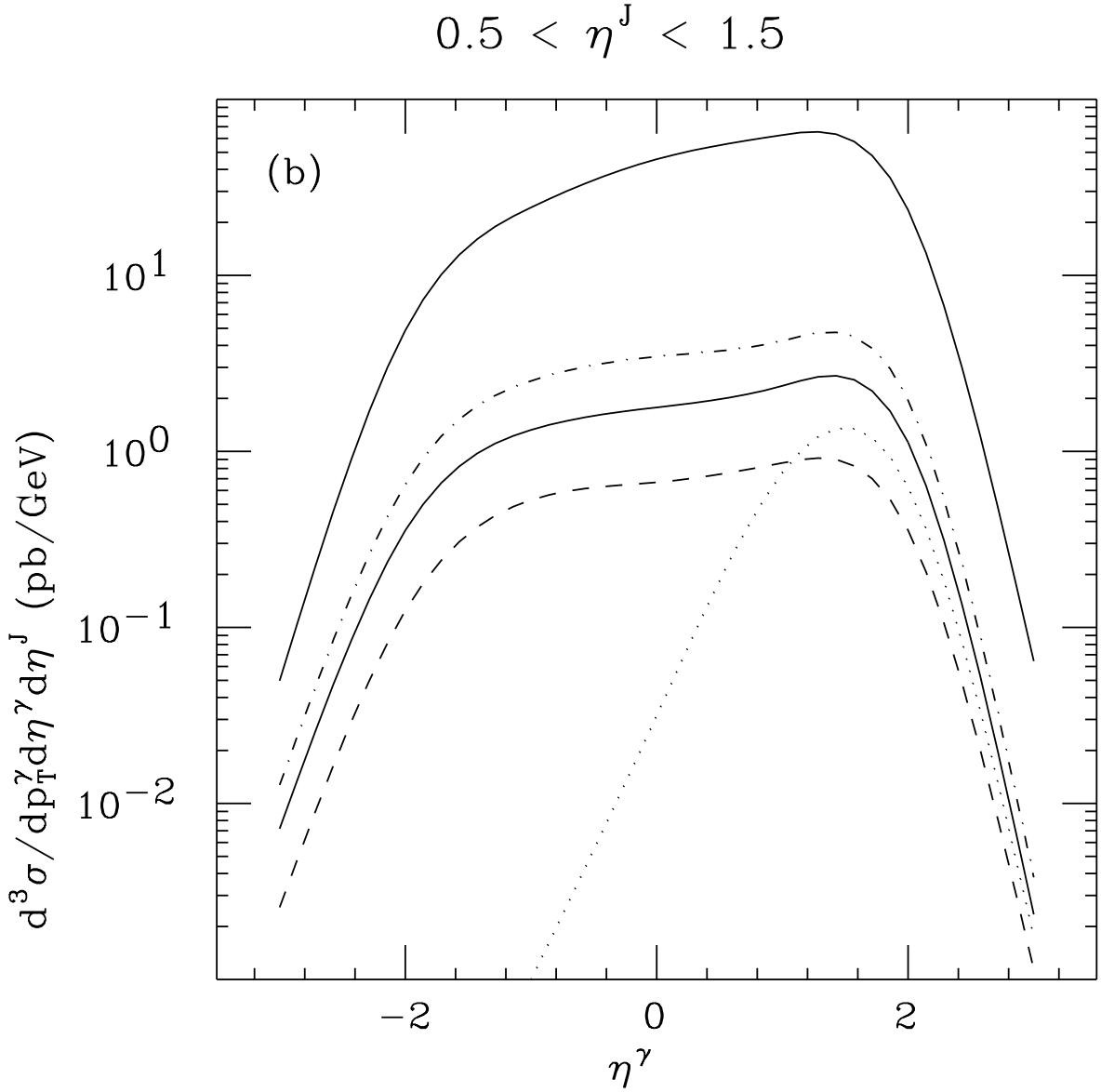
$0.5 < \eta^J < 1.5$
(b)
10^1
10^0
10^{-1}
10^{-2}
$d^3\sigma/dp_T^\gamma d\eta^\gamma d\eta^J$ (pb/GeV)
−2
0
2
η^γ

Fig. 2b

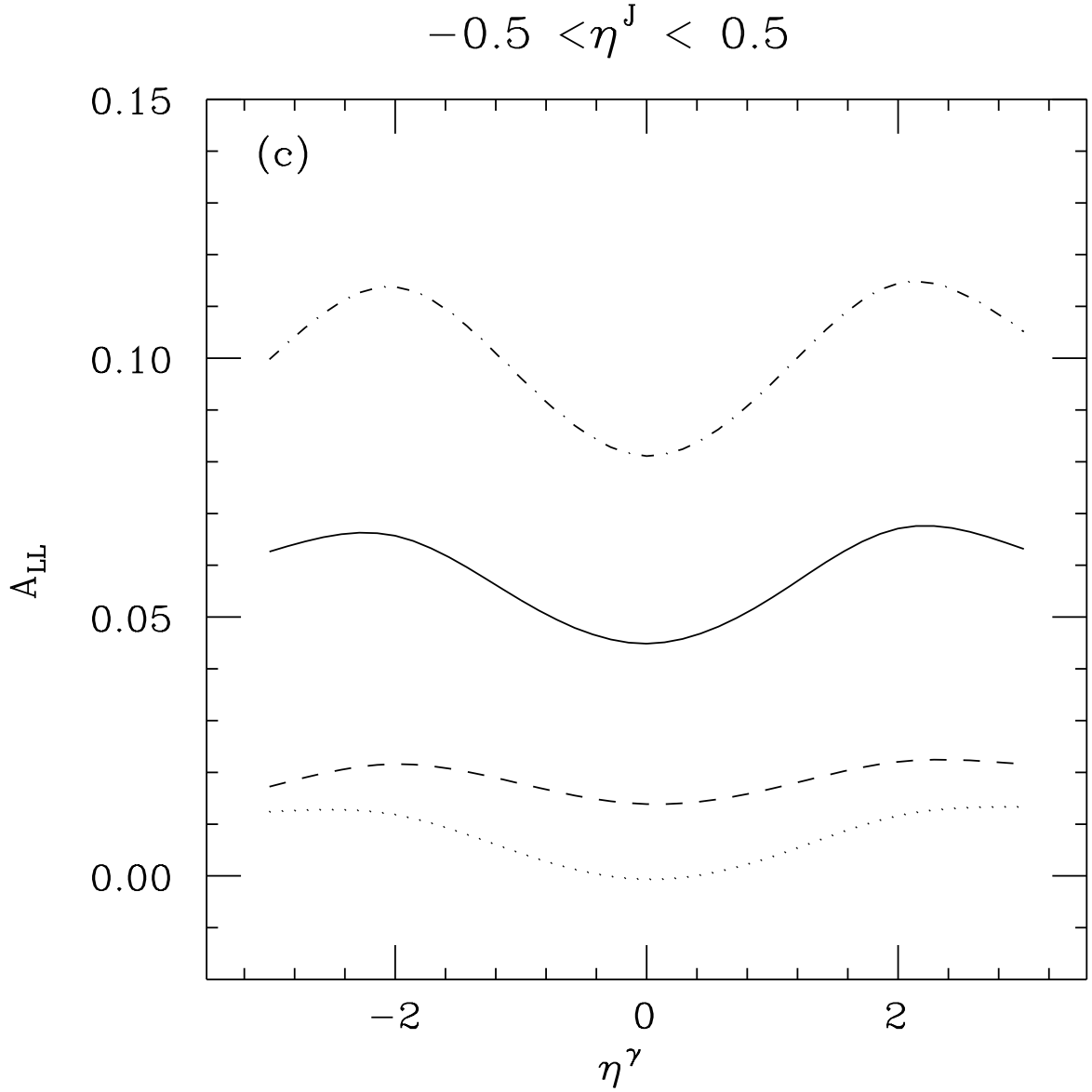

Fig. 2c

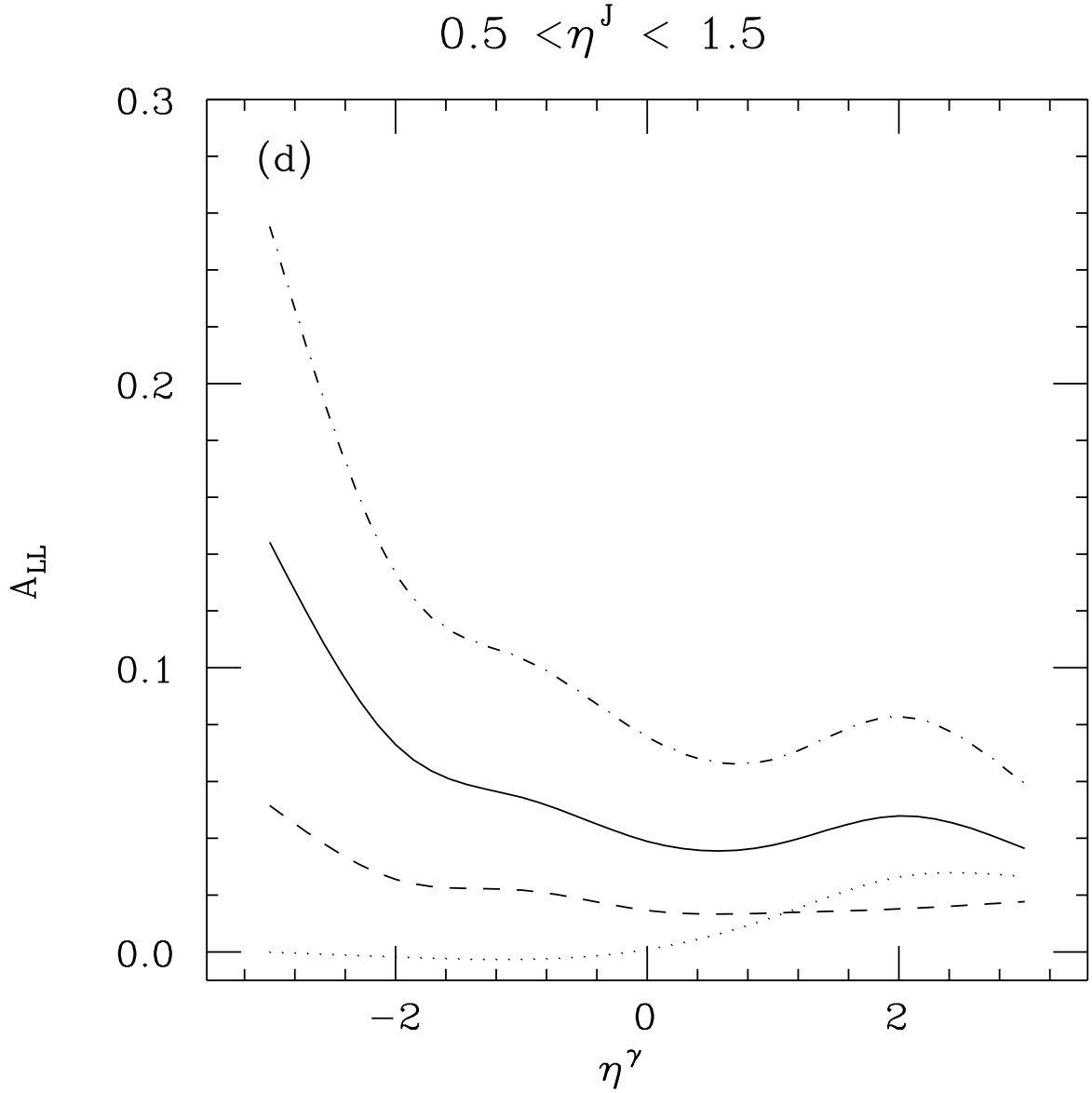

Fig. 2d

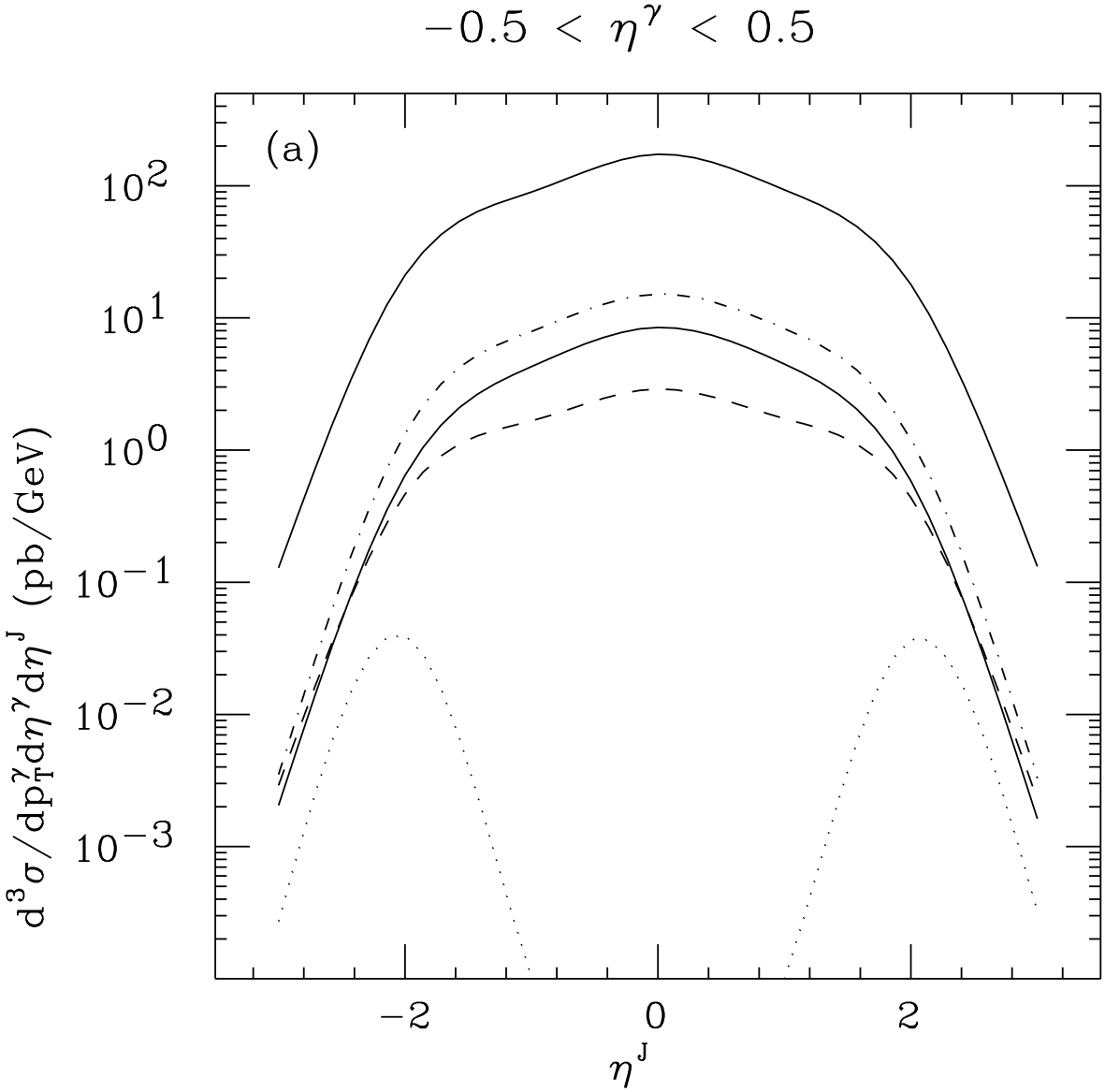
$-0.5 < \eta^\gamma < 0.5$
(a)
10^2
10^1
10^0
10^{-1}
10^{-2}
10^{-3}
$d^3\sigma/dp_T^\gamma d\eta^\gamma d\eta^J$ (pb/GeV)
−2
0
2
η^J

Fig. 3a

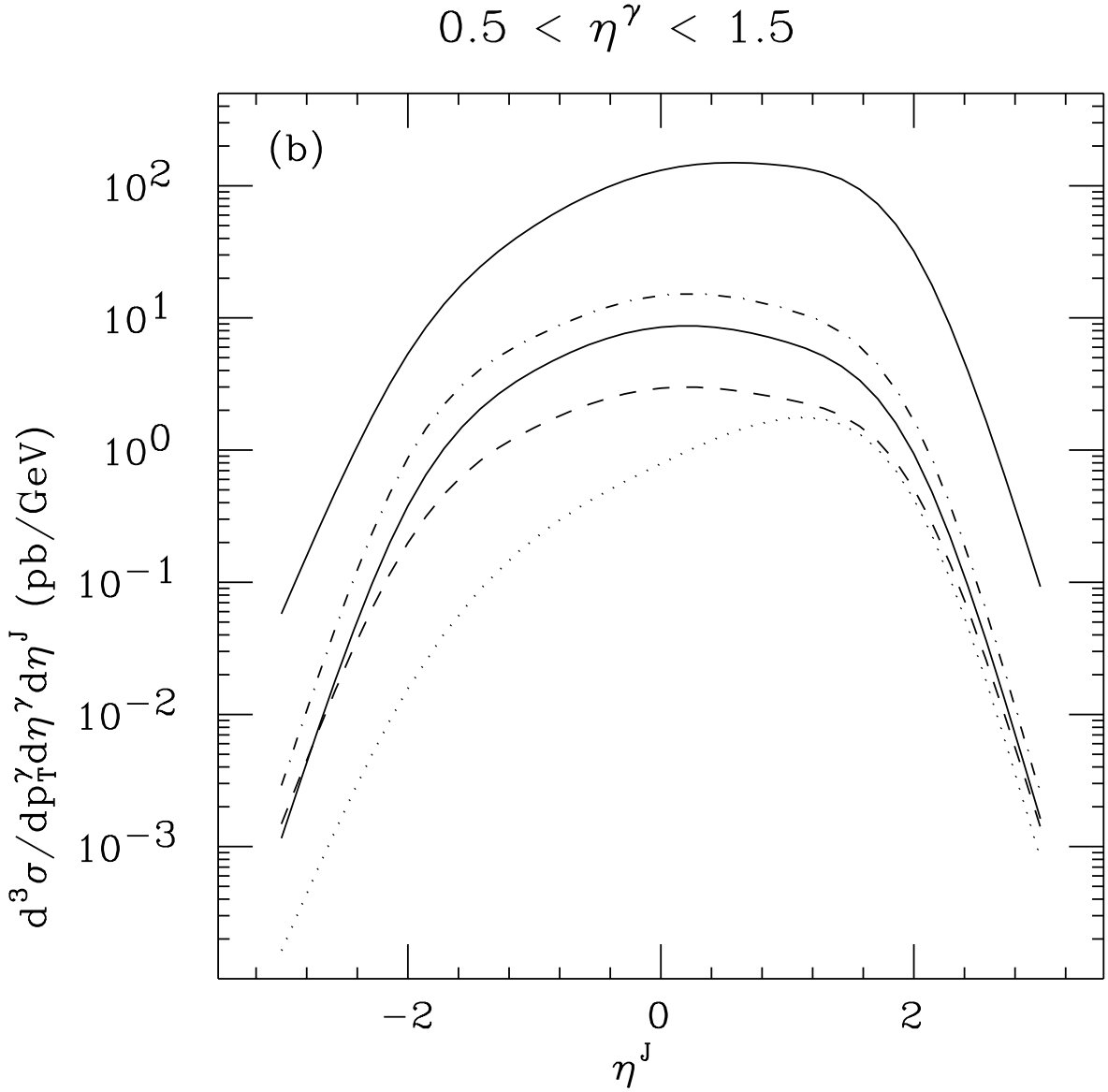
$0.5 < \eta^\gamma < 1.5$
(b)
10^2
10^1
10^0
10^{-1}
10^{-2}
10^{-3}
$d^3\sigma/dp_T^\gamma d\eta^\gamma d\eta^J$ (pb/GeV)
−2
0
2
η^J

Fig. 3b

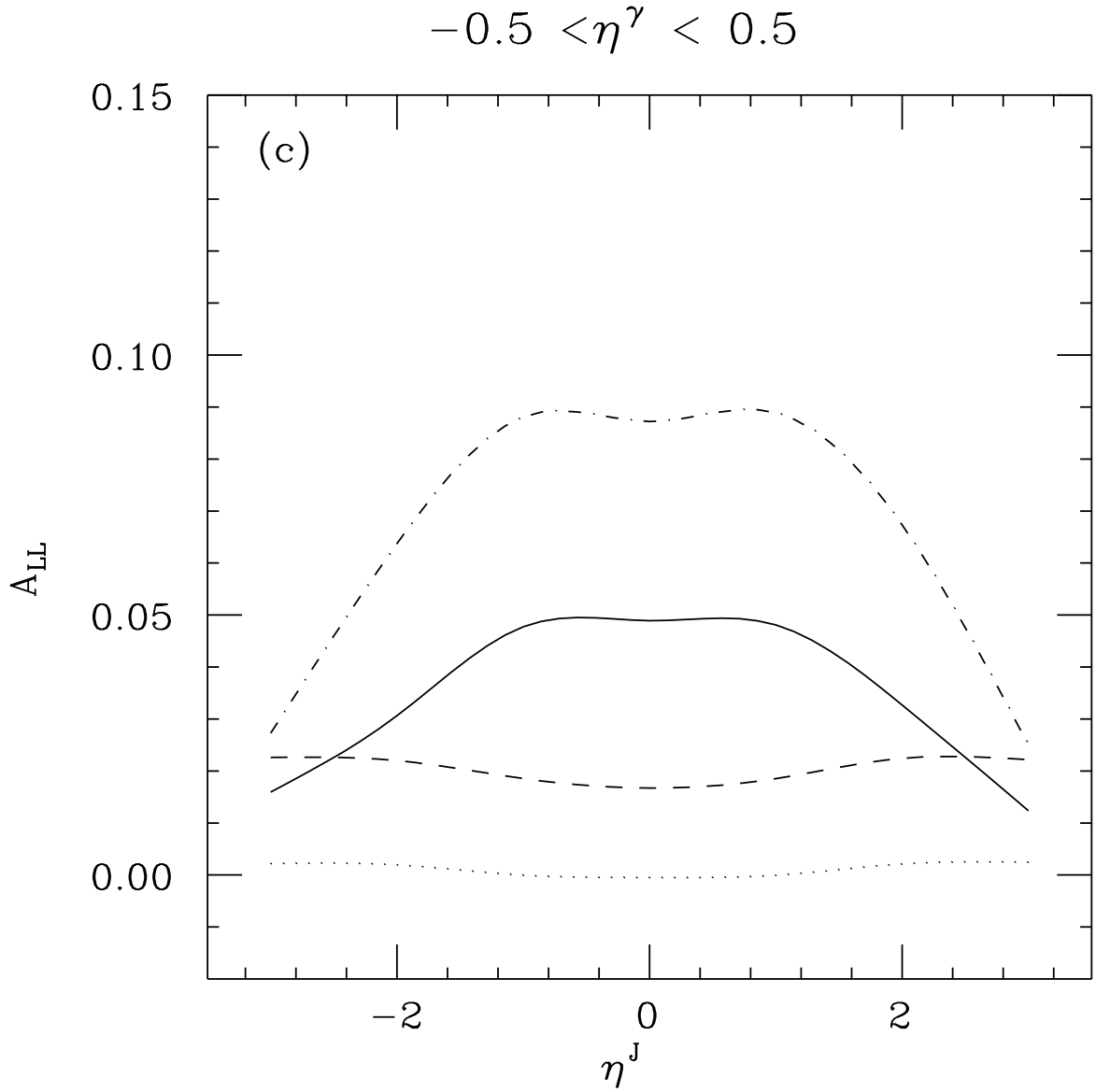

Fig. 3c

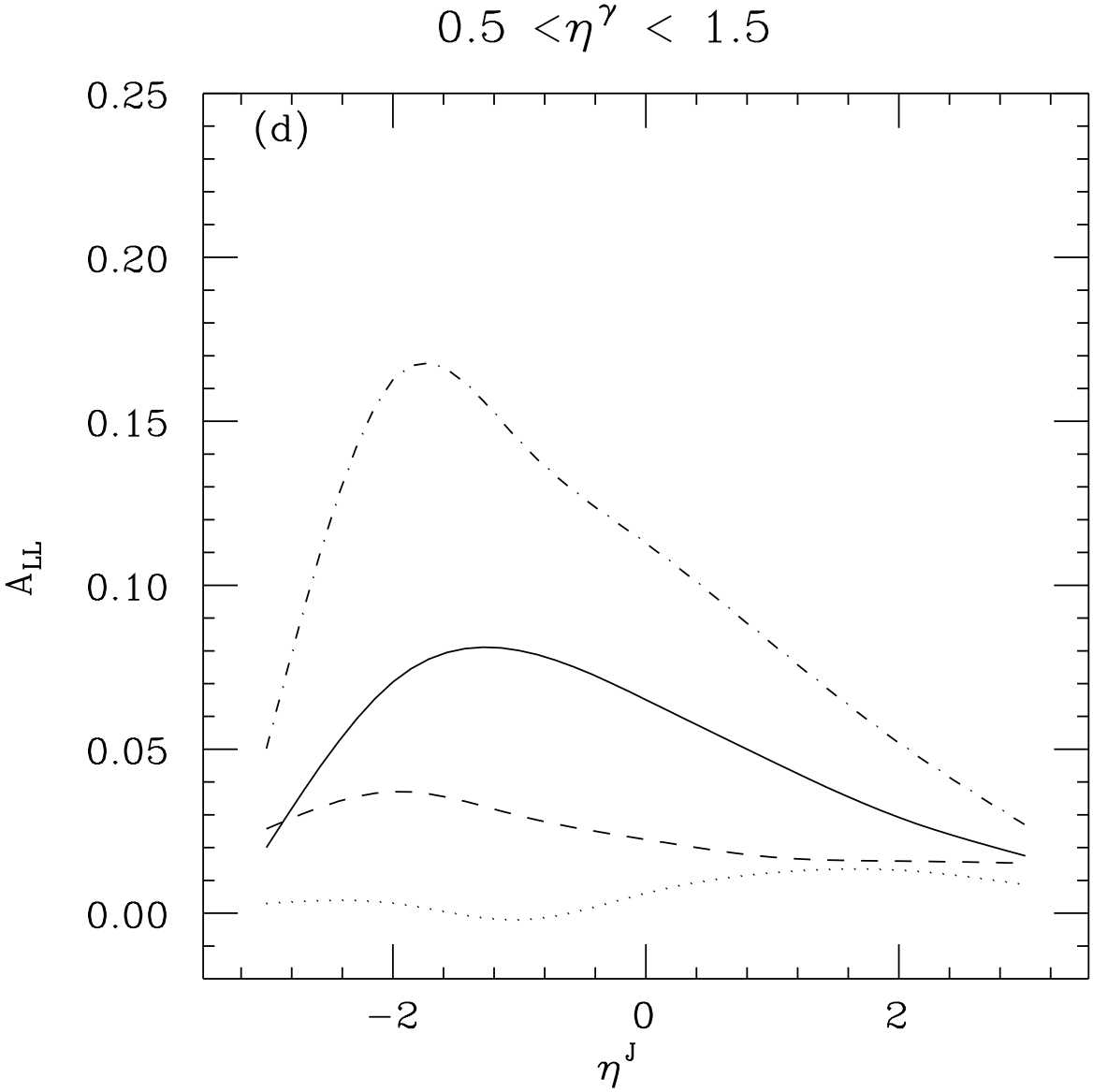

Fig. 3d

FIG. 4.